CHARACTERIZATION OF MANGANESE-CONTAINING Co-W COATINGS ELECTRODEPOSITED FROM ELECTROLYTES WITH VARIOUS ORGANIC COMPLEXING AGENTS

G. Tsurtsumia[1], N. Nioradze[1*], T. Lezhava[1], N. Koiava[1], P. Nikoleishvili[1], N. Jokhadze[1], R. Kurtanidze[1], G. Gorelishvili[1], B. Godibadze[2]

[1]Ivane Javakhishvili Tbilisi State University, R. Agladze Institute of Inorganic Chemistry and Electrochemistry, 11 Mindeli Str., Tbilisi 0186, Georgia
[2]F. Tavadze Institute of Metallurgy and Materials Science, 8b E. Mindeli Str., Tbilisi 0186, Georgia
**e-mail: nikoloz.nioradze@tsu.ge*

Received 14.05.2025
Accepted 22.08.2025

Abstract: *Galvanic coatings of Co-Mn are promising materials for obtaining protective spinel layers of $(Mn,Co)_3O_4$ on stainless steel, which can be successfully used in solid-oxide fuel cells (SOFCs) as interconnects. To enhance the anti-corrosion and heat resistance properties of Co-Mn, tungsten is introduced into the coatings via electrodeposition. Mn-containing Co-W coatings electrodeposited from electrolytes containing various non-toxic organic complexing agents show a shiny appearance are roughly 5 μm in thickness, have strong adherence to electrodes, and have uniformly incorporated oxygen. We found pH and current density dependence of Mn-containing Co-W coating content in an electrolyte containing a sodium citrate-EDTA complexing agent. X-ray structural analysis indicates that the Mn-containing Co-W coatings are likely amorphous, consisting of an α-Co solid solution with disordered dissolution of W and Mn. The corrosion potential E_{cor} of Mn-containing Co-W coatings deposited on a graphite cathode in a 3.5% aerated NaCl solution is -0.530 V (Ag/AgCl).*

Keywords: *Co-Mn/Co-W galvanic coatings; $(Mn,Co)_3O_4$ spinel layers; Solid-oxide fuel cells (SOFCs); Tungsten electrodeposition; Amorphous α-Co solid solution.*
DOI: 10.65382/2221-8688-2026-4-553-569

Introduction

Galvanic coating alloys of manganese with cobalt, nickel, zinc, copper, and others are characterized by high anti-corrosion properties and are considered as protective coatings for steel materials [1-4]. The presence of manganese with a high negative standard potential ($E^0_{Mn2+/Mn}$= -1.18 V, SHE*)* in the alloy provides corrosion protection for steels, as it acts as a "sacrificial" anode. Despite the relative abundance of metallic manganese, its galvanic coatings are not used to protect steels from corrosion [5-12]. This is due to the high chemical reactivity of manganese with oxygen and atmospheric moisture, as well as brittleness associated with short-term modification changes in crystals. Unlike galvanic coatings of pure manganese, coatings of its alloys are considered among the best and relatively inexpensive materials for anti-corrosion protection of steel [13-15].

Among the manganese-containing alloys obtained by electrodeposition, Co-Mn galvanic coatings are of particular interest, as they represent a promising material for internal contact with electrodes in solid oxide fuel cells (SOFCs) [16-19]. On the surface of the ferritic stainless steel used for this purpose, the buildup of an oxide layer and high volatility of Cr(VI) lead to failure of the element. This phenomenon can be prevented by applying a protective layer of highly conductive spinel $(Mn, Co)_3O_4$ on the stainless steel, obtained through high-temperature (900 °C) treatment of the electrodeposited Co-Mn coating.

Based on the practical interest in using Co-Mn coatings, we aimed to introduce a third component, tungsten, into the coating via electrodeposition, thereby obtaining a galvanic coating of the ternary Co-W-Mn alloy**.** It is known from the literature that enriching the surface layer of steel with W enhances its anti-

corrosion properties, wear resistance, and heat resistance at high temperatures, making it an alternative to chromium coatings [20, 21].

Obtaining galvanic coatings of alloys containing high melting point metals such as W, Mo, and Re is possible only with iron group metals (Fe, Co, Ni), a phenomenon often called induced co-precipitation [22]. The phenomenon of induced co-precipitation has been known for over 50 years, but the mechanism of this process is still not fully understood [23, 24]. Because of this, it is still impossible to predict the composition of the coating, and therefore its properties, based on the electrochemical characteristics of individual components.

An important factor for achieving the goal of our work was the presence of one of the metals of the iron triad - Co, which forms galvanic coatings with W. There are numerous data in the literature on the deposition of Co-W coatings [25-33]. Such coatings are in demand in the electrical and radio engineering industries. They have good catalytic properties, especially interesting in the technology of hydrogen production [34-36]. Researchers have shown increased interest in Co-W coatings and other W-containing thin galvanic coatings, since their magnetic properties differ sharply from the magnetic properties of the bulk material [37].

Organic complexing agents, mainly citric acid, its salt sodium citrate, and sodium gluconate, are important components in the composition of electrolytes used for electrodeposition of coatings. This is due to the poor solubility of sodium tungstate (a source of tungsten) in cobalt sulfate solutions. Importantly, the presence of a complexing agent, along with improved solubility, contributes to the alignment of electrodeposition potentials of metals. A number of authors believe that the complexation factor has a significant effect on the process of obtaining alloy coatings [38, 39]. The authors [39] consider that the electrodeposition of Co-W alloy from a solution containing a gluconate ligand most likely occurs with the reduction of a mixed heterometallic cobalt-tungsten complex (the ratio of tungsten to cobalt is 1:1), as well as a cobalt-containing complex (not with tungsten) and hydrogen reduction reactions. The ratio of the rates of reduction reactions of these complexes determines mainly the composition of the coating, which in turn depends on some factors**,** and if these are not considered, it is difficult to predict the composition of the deposited alloy.

In the present work, the formation of manganese-containing Co-W coatings by the electrodeposition method was investigated for the first time, using electrolytes containing the above-mentioned complexing agents as well as electrolytes containing other non-toxic agent mixtures - malic acid, sodium citrate-malic acid, and sodium citrate with EDTA. The electrochemical activity of various electrolytes for electrodeposition of alloys was analyzed by recording cyclic voltammetry curves.

Based on the data of CVs, the influence of the parameters of electrolysis - cathodic current density, electrolyte composition, and pH - on current efficiency, chemical composition, and morphology was studied**.** The coating thickness was also measured, and its appearance was assessed visually.

Experimental part

Electrolytes. The electrodeposition experiments were carried out in an electrolyte prepared using distilled water. All chemical reagents used were chemically pure and provided by Sigma-Aldrich. The pH of the electrolyte was adjusted by adding 40% H_2SO_4 or saturated NaOH solution. For the electrodeposition of Co-W-Mn alloy coatings, it was necessary to add complexing agents to the electrolyte - sodium citrate ($Na_3C_6H_5O_7 \cdot 5.5H_2O$), sodium gluconate ($C_6H_{11}NaO_7$), malic acid ($C_4H_6O_5$), and their mixtures, since sodium tungstate (the source of W) is poorly soluble in an aqueous solution of cobalt, manganese, and ammonium sulfates. To prepare the electrolyte with a specific composition, $CoSO_4 \cdot 7H_2O$ was first dissolved in distilled water under intense stirring, followed by the complexing ligand. After their dissolution, $Na_2WO_4 \cdot 2H_2O$, $MnSO_4 \cdot H_2O$, $(NH_4)_2SO_4$, and finally, surfactants such as acrylamide (C_3H_5NO) or but-2-yne-1,4-diol ($C_4H_6O_2$) were added successively. The latter is widely used to obtain high-quality, mirror-surfaced nickel coatings.

After adjusting the pH of the electrolyte, the solutions remain stable. Depending on the nature of the complexing agent, the color changes from dark violet to dark reddish.

Electrolysis and electrodes. A Plexiglas electrolyzer was used for electrodeposition. 0.5 L of the test electrolyte was circulated using a micropump (330 mL·min^{-1}) through a small intermediate circulation tank connected to the electrolyzer using silicone tubes. A glass electrode of a pH meter (MP512, China) was placed in the intermediate tank to record the pH and temperature of the electrolyte. To maintain a constant pH, 40% H_2SO_4 or saturated NaOH solution was added to the circulation tank, and the temperature was maintained by an electric heater placed in a quartz tube inserted into the circulation tank.

At the initial stage of the research, coatings were obtained on copper plate cathodes with dimensions of 2.0 × 1.0 × 0.015 cm, with both sides as working surfaces, with a total area of S ≈ 4.0 cm². In the later stages, graphite was mainly used as a cathode material in the experiments, which, unlike copper cathodes, has a number of advantages: chemical inertness, virtually no effect on the structure of the deposited alloy, and, most importantly, X-ray fluorescence analysis allows quick and accurate determination of the coating's chemical composition. Additionally, the hydrogen overpotential on the graphite cathode is relatively high, enabling the use of high current densities. High-purity, low-ash (ash content <0.03%) graphite from ГМЗ (Russia) with an area of 4 cm² was used for electrodeposition. The ratio of the cathode area to the solution volume (S/V) was 0.08 dm²·L^{-1}. For electrolysis, the test electrolyte was used once. Electrodeposition was carried out at cathode current densities of 0.05, 0.125, 0.2, and 0.25 A·cm^{-2}; the duration of each experiment was 15 minutes. The cathodes were polished with silicon carbide papers of different grades, up to 2000, until a mirror finish was achieved. The non-working part of the cathode was covered with epoxy resin. Before placing **it** in the electrolyzer, the graphite was treated with diluted sulfuric acid, then washed with distilled water and dried in air to a constant weight. In the electrolyzer, the cathode was placed between two identically sized (5 × 4 cm) grid-shaped titanium anodes at a distance of 3 cm. The surfaces of the anodes were modified with TiO_2-RuO_2 oxides (DSA electrodes), with a total area of 40 cm².

Preparation and characterization of coatings. To perform electrodeposition in galvanostatic mode, a DC power supply PE 1018-2 15V/30A (Plating Electronic GmbH, Germany) was used, which recorded the current, voltage change, and the amount of electricity passed (A·h). The electrodeposition time was 15 minutes, after which the cathode was removed from the electrolyzer while maintaining current supply and treated with a 10% potassium dichromate solution for 6-8 seconds. Without this procedure, manganese-containing coatings would turn blackish due to oxidation in air.

Subsequently, the coating on the cathode was washed with running and distilled water and finally dried with warm (50 °C) air. The alloy current efficiency (Φ_{Alloy}) was calculated gravimetrically from the change in mass of the coating deposited on the cathode (Δm) according to [40]:

$$\Phi_{Alloy} = \Delta m / (I \cdot \tau \cdot q_{alloy}) \cdot 100\% \qquad (1)$$

I - current, A
τ - time of electrolysis, h
q_{alloy} - electrochemical equivalent of the alloy:

$$q_{alloy} = 1/(\omega_{Co}/q_{Co} + \omega_W/q_W + \omega_{Mn}/q_{Mn}), \qquad (2)$$

where ω_{Co}, ω_W, ω_{Mn} and q_{Co}, q_W, q_{Mn}, are the mass fractions and electrochemical equivalents of Co, W, and Mn, respectively are:

$$q_{Co} = 1.099 \text{ g } (A \cdot h)^{-1}, \; q_W = 1.143 \text{ g } (A \cdot h)^{-1}, \; q_{Mn} = 1.025 \text{ g } (A \cdot h)^{-1}$$

Microphotography and elemental analysis of the coating surfaces were performed using a Hitachi TM3030 Plus scanning electron microscope (Japan).

Local composition analysis was conducted using an energy-dispersive X-ray spectrometer (EDS). The measurement error was ±1.2 wt%.

X-ray diffraction (XRD) analysis was performed on a ДРОН-4.07 diffractometer (Russia) using Ni-filtered $Cu_{k\alpha}$ radiation (λ = 1.54184 Å). The operating parameters were 40 kV tube voltage and 20 mA tube current. During measurements, samples were rotated in-plane using a ГП-13 goniometer.

Coating thickness was measured using a DCFN 3000 EZ instrument (accuracy: ±1 μm).

Electrochemical measurements. For electrochemical measurements, we used a CHI1140C potentiostat (CH Instruments Inc., USA). Voltammetric measurements were carried out in a standard three-electrode electrochemical cell. Cyclic voltammetry curves were recorded in aerated, stagnant solutions using a graphite working electrode (surface area = 0.1 cm²) with a freshly treated surface. The working electrode was connected to a saturated silver/silver chloride (Ag/AgCl) reference electrode via a Luggin capillary and salt bridge, separated by a glass valve.

The auxiliary electrode, a platinum plate (surface area = 5 cm²), was isolated from the working electrode by a glass filter.

To determine the electrochemical processes occurring at specific potentials on the graphite electrode in various electrolytes, CV curves were recorded at a potential scan rate of 10 $mV \cdot s^{-1}$. The scans were performed from the open-circuit potential (OCP) at 0.0 V in the cathodic direction to −1.7 V vs. Ag/AgCl and back.

According to the cyclic voltammogram obtained from the background electrolyte (Fig. 1, curve 1), hydrogen evolution becomes noticeable at -1.3 V. In the CV curve recorded from electrolytes containing $MnSO_4$-Na_2WO_4 (Fig. 1, curve 2), no peaks corresponding to the reduction or oxidation of Mn^{2+} or WO_4^{2-} are observed. On the graphite cathode, only intense hydrogen gas evolution occurs, which begins at -1.58 V. However, when scanning the potential in the anodic direction, a low-intensity cathodic wave is recorded at -1.17 V. This phenomenon appears to be related to the inner-sphere reduction reaction of tungsten-containing complex associates in solution, occurring on the cathode surface without metal deposition [39].

Results and discussion

Cyclic voltammograms. The CV curves were recorded on graphite cathodes in background electrolytes containing Na_2SO_4 and $MnSO_4$-Na_2WO_4 (Fig. 1), as well as in electrolytes containing $CoSO_4$ and $CoSO_4$-Na_2WO_4 (Fig. 2), and $CoSO_4$-$MnSO_4$-Na_2WO_4 (Fig. 3). The electrolytes contained the complexing agent DL-malic acid.

In electrolytes containing $CoSO_4$ and the complexing ligand DL-malic acid (without tungstate), intense hydrogen evolution is preceded by a cathodic peak corresponding to the reduction of Co^{2+} to metallic cobalt at -1.08 V (Fig. 2, curve 1). At higher cathodic potentials (approximately -1.2 V), the hydrogen evolution rate increases, as evidenced by noticeable current pulsations on the CV curve. Upon reversing the potential scan to the anodic direction, an anodic peak (i_a) corresponding to the dissolution of metallic cobalt deposited on the cathode is observed at -0.11 V. The shape of the CV curve obtained with the simultaneous presence of CoSO4 and Na_2WO_4 in the electrolyte shows that during preparative electrolysis, the electrodeposition of the Co-W alloy on the graphite cathode occurs at this potential. This process represents so-called "induced" co-precipitation, where the reduction of tungsten to the metallic state occurs immediately when the cobalt deposition potential is reached [22].

When scanning in the cathodic direction, the CV curve (Fig. 2, curve 2) reveals:

1. Anodic dissolution of the deposited coating starting at -0.68 V,
2. Increasing cathodic current densities across a wide range of cathodic potentials, and
3. A distinct cathodic peak for Co^{2+} reduction at -0.88 V.

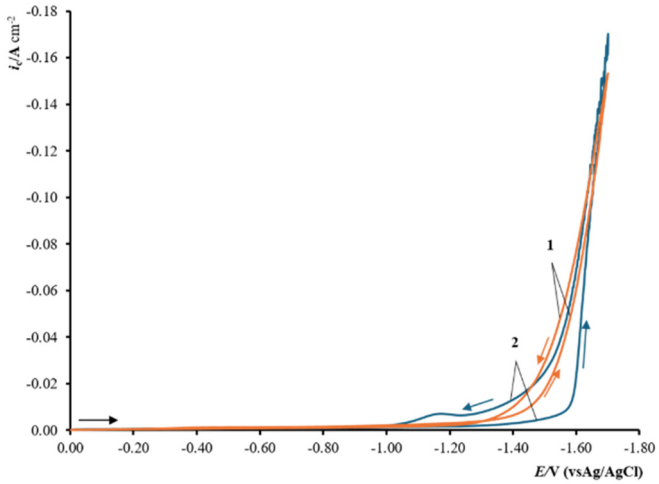

Fig. 1. Cyclic voltammograms (scan rate 10 mV s^{-1}, t=30 °C) on a graphite electrode in electrolytes (pH 5.5). Electrolyte composition, mol L^{-1}: (1) 0.5 Na_2SO_4; (2) 0.1$MnSO_4$ + 0.1 DL-Malic acid + 0.025 Na_2WO_4 + 0.15 $(NH_4)_2SO_4$ + 0.3 Na_2SO_4 + 0.0014 C_3H_5NO

Using the electrolyte (Fig. 2, curve 2) practically repeats the shape of the CV curve obtained without tungstate.

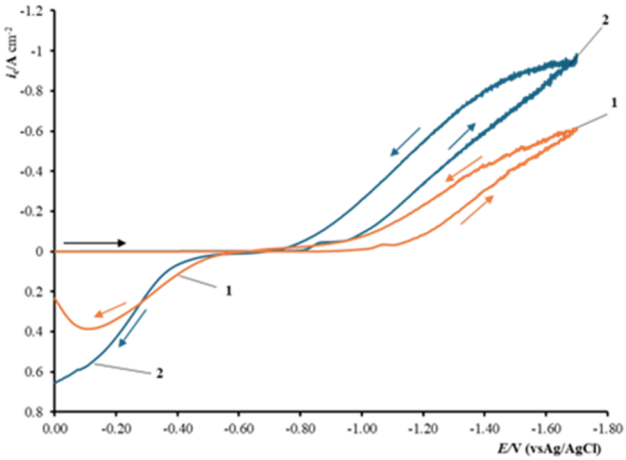

Fig. 2. Cyclic voltammograms (scan rate 10 mV s^{-1}, t=30 °C) on a graphite electrode in electrolytes (pH 5.5). Electrolyte composition, mol L^{-1}: (1) - 0.1$CoSO_4$ + 0.1 DL-Malic acid + 0.15$(NH_4)_2SO_4$ + 0.3Na_2SO_4 + 0.0014 C_3H_5NO; (2) - 0.1$CoSO_4$ + 0.1 DL-Malic acid + 0.15$(NH_4)_2SO_4$ + 0.3Na_2SO_4 + 0.0014 C_3H_5NO + 0.025 Na_2WO_4

In electrolytes containing $CoSO_4$, Na_2WO_4, and $MnSO_4$, the obtained CV curves (Fig. 3, curve 1) show a sharp increase in cathodic current density starting from -0.96 V. However, unlike the CV curve obtained in the electrolyte without Mn^{2+}, this curve does not exhibit a cathodic peak for Co^{2+} reduction. The electrodeposition of Co-W at -1.2 V was confirmed by preparative electrolysis.

At high cathodic potentials (starting from -1.4 V), the hydrogen evolution rate increases, which is attributed to the formation of Co and W atoms in the coating. These metals exhibit low overpotential for the hydrogen reduction reaction, particularly in the presence of tungsten. Consequently, the measured current is predominantly (91-95%) due to hydrogen reduction.

When scanning the cathode potential from -1.7 V in the anodic direction, the CV profile shows an anodic oxidation peak of the deposited alloy at -0.38 V. At relatively low cobalt concentrations in the electrolyte (Fig. 3, curve 2), the rates of reduction and oxidation processes are reduced, as evidenced by lower cathodic and anodic current densities at their respective potentials.

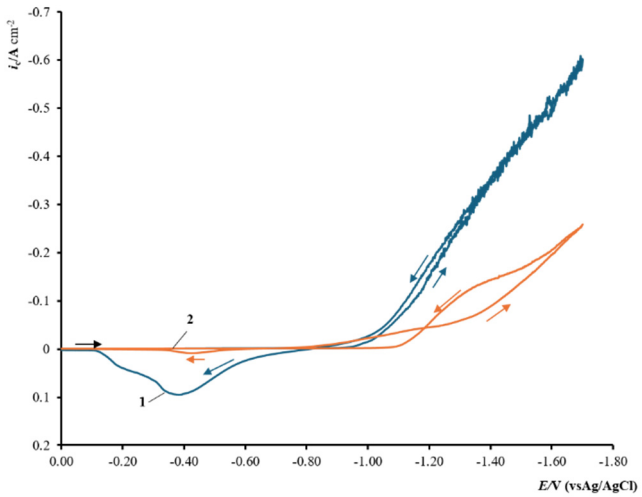

Fig. 3. Cyclic voltammograms (scan rate 10 mV s^{-1}, t=30°C) on a graphite electrode in electrolytes (pH 5.5). Electrolyte composition, mol L^{-1}: (1) - 0.1$CoSO_4$ + 0.1DL-Malic acid + 0.025Na_2WO_4 + 0.1$MnSO_4$ + 0.15 $(NH_4)_2SO_4$ + 0.3Na_2SO_4 + 0.007 But-2-yne-1,4-diol; (2) - 0.05$CoSO_4$+ 0.1DL-Malic acid + 0.025Na_2WO_4 + 0.15$MnSO_4$ + 0.15$(NH_4)_2SO_4$ + 0.3Na_2SO_4 + 0.007 But-2-yne-1,4-diol

CV curves of similar shapes were obtained in electrolytes containing $CoSO_4$-$MnSO_4$-Na_2WO_4 with various complexing agents (Fig. 4).

The effect of pH on coating electrodeposition was studied in an electrolyte containing a sodium citrate-EDTA complexing agent mixture, as these coatings exhibited greater mass deposition per unit charge and higher manganese content (see Section 3.3) compared to other complexing agents.

From CV curves recorded at pH 3.5 and 5.5 in the sodium citrate-EDTA electrolyte (Figs. 5 and 6), it is evident that:

- In the more acidic electrolyte (pH 3.5), cathodic scanning shows significant current increase on the graphite cathode starting at -1.2 V
- At high cathodic potentials, current pulsations occur due to intense hydrogen evolution.

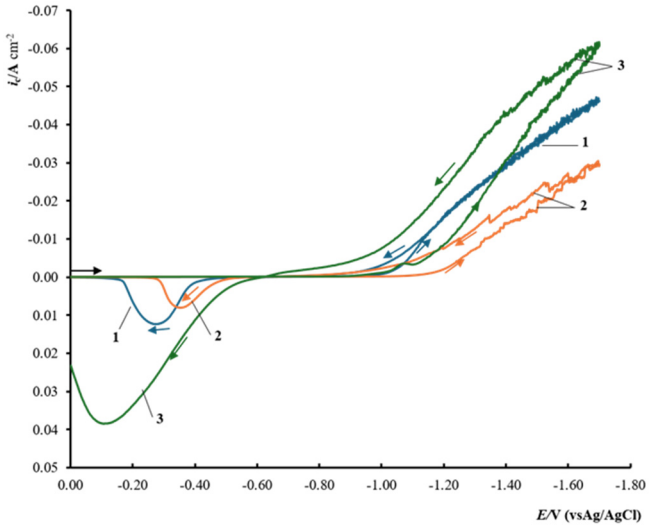

Fig. 4. Cyclic voltammograms (scan rate 10 mV s^{-1}, t=30°C) on a graphite electrode in electrolytes (pH 5.5). Electrolyte composition, mol L^{-1}: (1) - 0.1$CoSO_4$ + 0.1Na_2WO_4 + 0.5$MnSO_4$ + 0.5$(NH_4)_2SO_4$ + 0.007 But-2-yne-1,4-diol + 0.7 Gluconic acid sodium salts; (2) - 0.1$CoSO_4$ + 0.1Na_2WO_4 + 0.5$MnSO_4$ + 0.5$(NH_4)_2SO_4$ + 0.007 But-2-yne-1,4-diol + 0.1 Sodium citrate salts + 0.1DL-Malic acid; (3) - 0.1$CoSO_4$ + 0.1Na_2WO_4 + 0.15$MnSO_4$ + 0.2 $(NH_4)_2SO_4$ + 0.007 But-2-yne-1,4-diol +0.25 Sodium citrate salts + 0.04 Citric acid

After reversing the potential toward the anodic direction, the peak of anodic dissolution of the coating deposited on the cathode is recorded at -0.35 **V**. During repeated scanning of the potential in the cathodic region, the slope of the curve and the potential value of the anodic oxidation peak of the alloy remain unchanged, but the anodic oxidation current density increases slightly, likely due to the increased mass of alloy deposited during repeated cathodic polarization.

The shape of the CV curve recorded in the 3rd cycle remains consistent in subsequent cycles and shows practically no change. Similarly, relatively stable CV curves are obtained at pH 5.5 (Fig. 6).

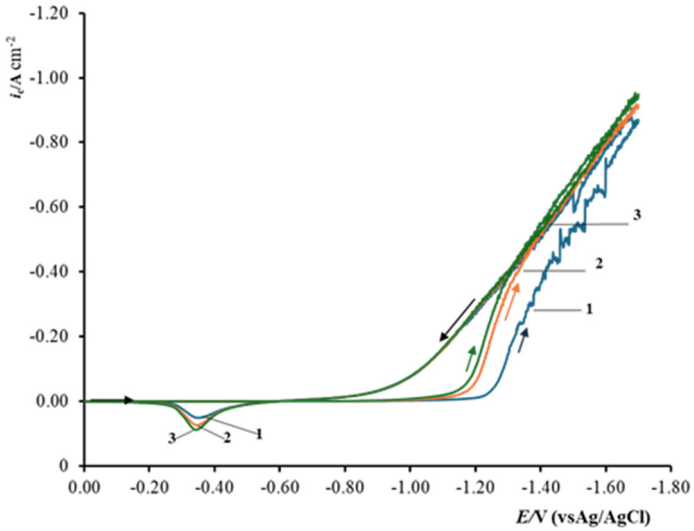

Fig. 5. Cyclic voltammograms (scan rate 10 mV s^{-1}, t=30°C) on a graphite electrode in electrolytes (pH 3.5). Electrolyte composition, mol L^{-1}: 0.15 $CoSO_4$ + 0.25 Sodium citrate salts + 0.1EDTA +0.1$Na_2WO_4 \cdot 2H_20$ + 0.5 $(NH_4)_2SO_4$ + 0.5 $MnSO_4$ + 0.007 But-2-yne-1,4-diol. CV The curves are recorded: 1 - during the first cycle; 2- during the second cycle; 3 - in the third cycle

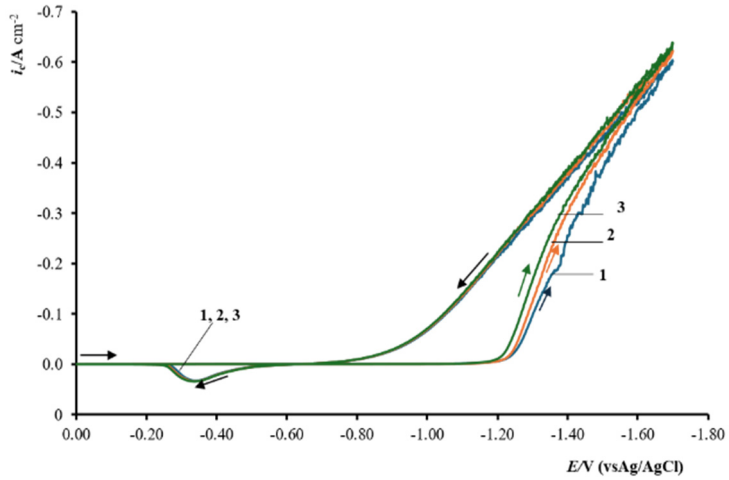

Fig. 6. Cyclic voltammograms (scan rate 10 mV s^{-1}, t=30°C) on a graphite electrode in electrolytes (pH 5.5). Electrolyte composition, mol L^{-1}: 0.15 $CoSO_4$ + 0.25 Sodium citrate salts + 0.1 EDTA +0.1 Na_2WO_4 + 0.5 $(NH_4)_2SO_4$ + 0.5 $MnSO_4$ + 0.007 But-2-yne-1,4-diol. CV The curves are recorded: 1- during the first cycle; 2-during the second cycle; 3- in the third cycle

On the CV curve recorded on the graphite cathode, for the 1st cycle, at high cathodic potentials, a current pulsation is noticeable, which is not observed on the curves of repeated cycles. But unlike the voltammogram obtained at pH 3.5, the magnitude of the anodic oxidation potential and current density at pH 5.5 is constant and repeats even after several repetitions of the potential scan. It should be noted that at pH 3.5, in contrast to the curves obtained at pH 5.5, the

cathodic current values are high due to the increased rate of hydrogen generation.

Thus, all recorded CV curves are characterized by increasing current density at high negative cathode potentials, which is associated with both alloy electrodeposition and simultaneous hydrogen gas evolution. The current efficiency for hydrogen evolution ranges between 91 and 95 %, resulting in correspondingly low current efficiency for alloy deposition.

Despite the similarity of the CVs, differences exist primarily in the anodic oxidation potential values of the coatings. These variations likely reflect the production of coatings with different compositions due to complex cathode processes.

Preliminary electrodeposition test. At the initial stage of the research, preliminary data on electrolyte composition and electrolysis parameters were obtained through test electrodeposition of binary Co-Mn alloy coatings. Electrolysis was performed in electrolytes containing cobalt-manganese sulfates (pH 3.5 and pH 5.5) without complexing ligands and, for comparison, in a reference electrolyte, which contained cobalt-manganese sulfates along with sodium gluconate as a complexing agent.

The test electrolytes contained small amounts of surfactants (acrylamide or butynediol) and ammonium sulfate as an additive. Ammonium sulfate, known from pure manganese electrolysis processes, prevents manganese hydroxide formation at the cathode while improving electrolyte conductivity. Tables 1 and 2 present the Co-Mn coating test results.

From Table 1, coatings with whitish bright appearance and 32-36 μm thickness (ω(Co):ω(Mn) = 1:1) were obtained from simple-composition electrolytes (25°C, pH 5.5) even without complexing agents, at 200-250 $mA \cdot cm^{-2}$ current density with approximately 50% current efficiency. These coatings, similar to previous reports, can form protective $(Mn,Co)_3O_4$ spinel layers on steel. For coatings from sodium gluconate-containing electrolytes (25°C, pH 5.5), the surface was shiny but with reduced thickness and current efficiency (Table 2). This likely results from stable cobalt-manganese gluconate complexes that reduce slower than hydrated ions at the cathode [16]. The tests demonstrated higher current efficiency at pH 5.5 versus pH 3.5, which guided subsequent electrolyte preparation for manganese-containing Co-W coatings.

Table 1. Experimental results of obtaining of manganese-containing Co-Mn coatings. Electrolyte composition, mol L^{-1}: $MnSO_4$ - 0.6, $CoSO_4$-0.1, $(NH_4)_2SO_4$-0.95, C_3H_5NO-0.0014; t=25 °C; Electrolysis time, τ=15min; Appearance of the coating- Light color.

The cathodic current density, i_c /mA cm^{-2}	The mass of alloy deposited on the cathode, m_{alloy}/g	Composition of the coating, ω(Me), Wt.%		Current efficiency, Φ_{alloy}/%	Thickness of the coating, δ/μm
		ω(Co)	ω(Mn)		
pH 3.5					
40	0.0225	96.8	3.2	51.27	7.5
75	0.0327	96.0	4.0	39.78	10.9
125	0.0467	78.8	21.2	34.59	15.17
200	0.054	75.5	24.5	25.0	17.4
pH 5.5					
40	0.0339	76.1	23.9	78.5	11.0
75	0.0515	73.9	26.1	64.0	17.0
125	0.0786	58.9	41.1	59.0	25.0
200	0.1045	51.1	48.9	49.5	32.0
250	0.1173	47.6	52.4	44.0	36.0

Table 2. Experimental results of obtaining of manganese-containing Co-Mn coatings. Electrolyte composition, mol L^{-1}: $MnSO_4$ - 0.6, $CoSO_4$-0.1, $(NH_4)_2SO_4$-0.95, C_3H_5NO-0.0014, $C_6H_{11}Na0_7$-0.7; t=25 ^{0}C; pH 5.5; Electrolysis time τ=15min; Appearance of the coating- Glittery.

The cathodic current density, i_c/ mA cm^{-2}	The mass of alloy deposited on the cathode, m_{alloy}/g	Composition of the coating, ω(Me)/ Wt.%		Current efficiency, Φ_{alloy}/%	Thickness of the coating, δ/μm
		ω(Co)	ω(Mn)		
40	0.0081	90.1	9.9	18.4	2.7
75	0.0125	76.0	24.0	15.4	4.0
125	0.0151	73,5	26.5	11.2	4.6
200	0.0187	66.2	33.8	8.7	4.9
250	0.0212	50.3	49.7	6.3	4.2

DC electrodeposition of manganese-containing Co-W alloys from different electrolytes. During the electrodeposition of manganese-containing Co-W alloys, primary focus was given to investigating how electrolyte composition and cathodic current density affect coating current efficiency, thickness, appearance, chemical composition, and morphology.

To enable sodium tungstate dissolution in cobalt-manganese sulfate electrolytes, the addition of complexing agents or their mixtures was required. Experimental results for Co-W-Mn coatings from various electrolyte compositions are shown in Tables 3 and 4. All electrolytes were prepared by dissolving reagents in distilled water following the sequence specified in the tables.

Table 3. Experimental results of obtaining of manganese-containing Co-W coatings from electrolytes containing various complexing agent during of electrolyzes 15 min, Temperature 25 °C. Appearance of the coating obtained in series of experiment #1*-unsatisfying, #1-2 was shiny, #3-light color.

Series of exp. #	Electrolyte composition/ mol L^{-1}	i_c /A cm^{-2}	m_{alloy}/g	ω(Me)/Wt.%; (at.%)				Φ_{alloy} /%	δ/μm
				ω(Co)	ω(W)	ω(Mn)	ω(O)		
1	$CoSO_4 \cdot 7H_2O$ 0.15 $Na_3C_6H_5O_7 \cdot 5.5H_2O$ 0.25 $Na_2H_2C_{10}H_{12}O_8N_2 \cdot 2H_2O$ 0.1 $Na_2WO_4 \cdot 2H_2O$ 0.1 $MnSO_4 \cdot H_2O$ 0.3 $(NH_4)_2SO_4$ 0.5 $C_4H_6O_2$ 0.014	pH 3.5							
		50*	-	-	-	-	-	-	-
		125	0.0068	69.38 (55.37)	14.31 (3.66)	3.36 (2.87)	12.96 (38.09)	8.9	4.6
		200	0.0096	73 (60.05)	10.5 (2.77)	5.97 (5.27)	10.53 (31.91)	9.65	5.3
		250	0.0102	71.74 (52.09)	6.5 (1.51)	6.22 (4.85)	15.54 (41.56)	11.4	5.7
2		pH 5.5							
		50	0.0072	43.73 (24.76)	19.84 (3.6)	2.93 (1.78)	33.51 (69.87)	9.3	4.9
		125	0.0086	49.95 (31.87)	21.5 (4.4)	2.03 (1.39)	26.52 (62.34)	9.55	5.3
		200	0.0098	64.66 (48.95)	16.54 (4.01)	2.73 (2.22)	16.07 (44.81)	10.7	5.8
		250	0.011	72.3 (59.75)	13.87 (3.67)	2.57 (2.27)	11.27 (34.31)	11.8	5.9
3	$CoSO_4 \cdot 7H_2O$ 0.1	pH 4.5							
		120	0.0065	67.58 (66.64)	24.68 (7.80)	0.99 (1.05)	6.75 (24.51)	4.18	3.8

	$Na_3C_6H_5O_7 \cdot 5.5H_2O$ 0.1	160	0.0099	70.95 (53.08)	12.16 (2.92)	1.31 (1.05)	15.58 (42.95)	4.7	4
	C4H605 0.1	200	0.0126	73.41 (62.38)	14.83 (4.04)	1.44 (1.31)	10.31 (32.27)	5.1	4.3
	$Na_2WO_4 \cdot 2H_2O$ 0.1 $(NH_4)_2SO_4$ 0.5 $MnSO_4 \cdot H_2O$ 0.3 $C_4H_6O_2$ 0.007	250	0.0159	73.79 (56.96)	11.2 (2.77)	1.2 (1.00)	13.81 (39.27)	5.3	4.95

From the data in Tables 3 and 4, it is evident that electrodeposition produces shiny but relatively thin coatings (~5 μm) with low current efficiency. These coatings exhibit strong adhesion to the cathode surface. Although some electrolytes contain Mn^{2+} concentrations five times higher than Co^{2+}, the manganese content in coatings reaches only 2.65 wt.% (except for the sodium citrate-EDTA electrolyte). At higher current densities ($i > 0.25$ A cm^{-2}), coating quality deteriorates, and current efficiency declines with prolonged electrolysis ($\tau > 20$ min). This aligns with cyclic voltammetry data, where high cathodic current densities simultaneously drive Mn-containing Co-W electrodeposition and intense hydrogen evolution. As noted earlier, this likely stems from metallic W inclusions in the coating, which lower hydrogen reaction overpotential, accelerating gas evolution and sharply reducing current efficiency. Such rapid efficiency loss is typical for Co-W alloy electrodeposition, as reported in literature [26, 28].

Table 4. Experimental results of obtaining of manganese-containing Co-W coatings from electrolytes containing various complexing agent during of electrolyzes 15 min, pH 5.0. Appearance of the coating obtained in series of experiments was shiny.

Series of exp. #	Electrolyte composition/ mol L^{-1}	i_c /A cm^{-2}	m_{alloy}/g	ω(Me)/Wt.%; (at.%)				Φ_{alloy}/ %	δ/μ m
				ω(Co)	ω(W)	ω(Mn)	ω(O)		
1	$CoSO_4 \cdot 7H_2O$ 0.1 $C_4H_6O_5$ 0.1 $Na_2WO_4 \cdot 2H_2O$ 0.025 Na_2SO_4 0.3 $(NH_4)_2SO_4$ 0.5 $MnSO_4 \cdot H_2O$ 0.1 $C_4H_6O_2$ 0.014	Temperature 30 °C							
		40	0.0043	75.17 (67.33)	15.86 (4,55)	0.62 (0.62)	8.34 (27.52)	8.8	3.7
		60	0.0055	79.12 (73.71)	13.98 (4.17)	0.65 (0.65)	6.26 (21.47)	7.7	4.9
		90	0.0077	74.09 (66.76)	16.33 (4.72)	1.39 (1.34)	8.19 (27.19)	7.1	4.9
		120	0.0086	74.55 (67.01)	15.75 (4.58)	1.93 (1.88)	7.76 (25.93)	5.9	5.5
2		Temperature 50 °C							

	$CoSO_4 \cdot 7H_2O$ 0.1 $C_6H_{11}NaO_7$ 0.7 $Na_2WO_4 \cdot 2H_2O$ 0.1 $(NH_4)_2SO_4$ 0.5 $MnSO_4 \cdot H_2O$ 0.5 $C_4H_6O_2$ 0.007	60	0.0061	84.5 (73.20)	6.15 (1.71)	2.09 (1.94)	7.26 (23.15)	8.57	3.5
		90	0.0125	82.06 (67.79)	6.49 (1.72)	2.01 (1.79)	9.43 (28.71)	11.45	4.2
		120	0.0169	83.17 (66.70)	4.06 (1.04)	2.62 (2.25)	10.16 (30.01)	11.6	4.7
		150	0.0192	87.08 (74.91)	3.43 (0.95)	2.63 (2.43)	6.85 (21.72)	10.8	5.2

Fig. 7 represents high-resolution SEM micrographs of coatings deposited on graphite from sodium citrate-EDTA electrolytes (pH 3.5 and 5.5) at 0.125, 0.2, and 0.25 A cm^{-2}.

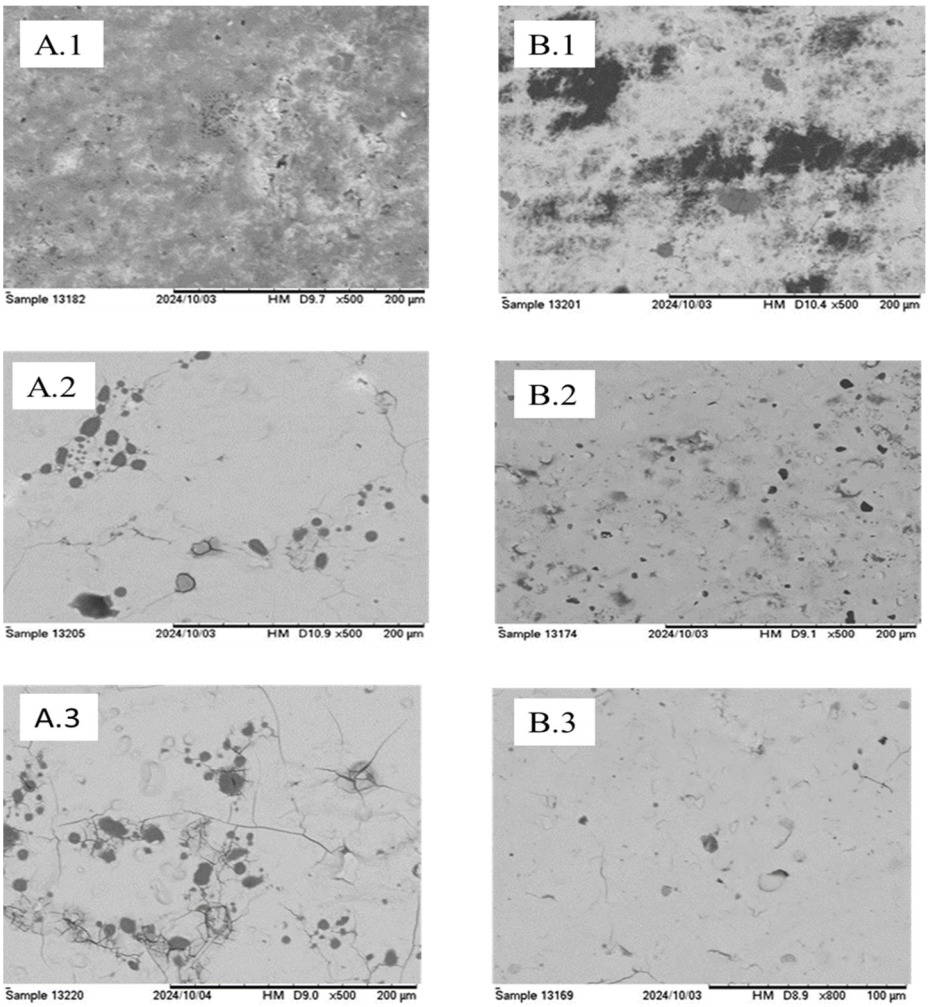

Fig. 7. SEM images of the surfaces of manganese-containing Co-W coatings obtained by electrodeposition from electrolytes containing a mixture of sodium citrate and EDTA on a graphite cathode at temperature of 30 °C.

A. pH 3.5: (A.1) i=0.125 A cm^{-2}; (A.2) i=0.2 A cm^{-2}; (A.3) i=0.25 A cm^{-2}

B. pH 5.5: (B.1) i=0.125 A cm^{-2}; (B.2) i=0.2 A cm^{-2}; (B.3) i=0.25 A cm^{-2}

While all coatings appear shiny, SEM reveals nonuniform component distribution and microcracks. Hydrogen evolution and cathode-layer alkalinization likely promote Co oxide/hydroxide formation and their incorporation into coatings. These inclusions, along with hydrogen adsorption, may inhibit crystallite growth. Consequently, coatings exhibit heterogeneous composition, with clusters of co-precipitated atoms and microvoids, potentially due to slow diffusion of dischargeable particles under inadequate hydrodynamic conditions.

The latter issue can be mitigated by employing pulsed electrolysis, which will be explored in future studies. The shiny coating surface likely results from intense light reflection off a smooth layer formed by adsorbed oxide-hydroxide particles on crystallite surfaces and their incorporation into the growing coating.

Table 5 summarizes the atomic composition (at.%) of coatings deposited on graphite electrodes at pH 3.5 and pH 5.5 across varying cathodic current densities.

Table 5. Dependence of the composition of the coatings deposited on graphite from electrolytes containing a mixture of sodium citrate and EDTA at pH 3.5 and pH 5.5 from the cathodic current density; t=30 °C; Electrodeposition time 15 min.

I_c/Acm^{-2}	Co, at.%	O, at.%	W, at.%	Mn, at.%
pH	3.5			
0.05	Coatings are bad quality			
0.125	55.37	38.09	3.66	2.87
0.2	60.05	31.91	2.77	5.27
0.25	52.09	41.56	1.51	4.85
pH	5.5			
0.05	24.76	69.87	3.60	1.78
0.125	31.87	62.34	4.40	1.39
0.2	48.95	44.81	4.01	2.22
0.25	59.75	34.31	3.67	2.27

All obtained coatings contained oxygen, likely as cobalt oxides/hydroxides. Table 4 data reveal that at pH 3.5, increasing cathodic current density reduces W content while elevating O and Mn levels, with Co remaining stable. Conversely, at pH 5.5, higher current densities increase Co and Mn but decrease O content, while W stays constant. The more predictable compositional trends at higher pH likely stem from reduced hydrogen evolution and weaker adsorption versus acidic conditions, promoting uniform deposition.

Microcracks correlate strongly with the incompletely understood complex mechanism of alloy electrodeposition. Per the radical-film theory [23, 24], tungstate ions in the cathode-adjacent layer (where high pH prevails) form electroactive heterometallic Co-W complexes with cobalt hydroxo-species {$CoOH^+$, $Co_4(OH)_4^{4+}$}. This process is complicated by concurrent water reduction, which alters local pH, triggering oxide/hydroxide formation and hydrogen evolution-both critically impacting coating composition and morphology.

Microcracks likely originate from Co oxide/hydroxide and hydrogen adsorption on growing crystallite faces, impeding discharged particles from integrating into the lattice. Consequently, small crystallites become isolated by hydroxides/hydrogen, preventing uniform surface coverage. Adding 5 mg·L^{-1} sodium dodecyl sulfate (SDS) to suppress hydrogen adsorption reduced but did not eliminate microcracks, even at 50°C. Notably, most literature-reported Co-based coatings (e.g., Co-Mn, Co-W [16-18, 20, 21] exhibit microcracks, typically remedied by heat treatment.

Co-W-Mn coatings demonstrate electrocatalytic activity (e.g., for hydrogen evolution [34-36]), primarily governed by their electrochemically active surface area (ECSA). The high ECSA of these alloys arises from their nanocrystalline/amorphous structure and defective morphology (pores, microcracks), which amplify surface area.

Structure of manganese-containing Co-W coatings. The coating diffractogram (Fig. 8) shows, in addition to graphite substrate peaks, broad diffraction maxima corresponding to (100), (002), and (101) planes of nearly amorphous α-Co. The α-Co grain size, calculated via the Scherrer equation using the (101) peak half-width (2θ ≈ 47°), does not exceed 5 nm. Notably, the α-Co (002) peak intensity (2θ ≈ 44.5°) significantly surpasses that of (101), suggesting a (002) texture-preferred grain orientation.

High background noise and weak radiation penetration, caused by strong Co fluorescence under Cu Kα radiation (λ=1.54184 Å), degraded diffractogram quality. Thus, additional XRD analysis was performed using Fe Kα radiation (λ=1.93728 Å) (Fig. 9). Despite improved sensitivity/resolution, the β-Co (200) peak remained indistinct, and no separate peaks for W, Mn, or other crystalline phases were detected, likely due to their disordered dissolution in α-Co.

XRD results confirm that electrodeposited Mn-containing Co-W coatings consist primarily of an amorphous α-Co solid solution with randomly distributed W and Mn atoms.

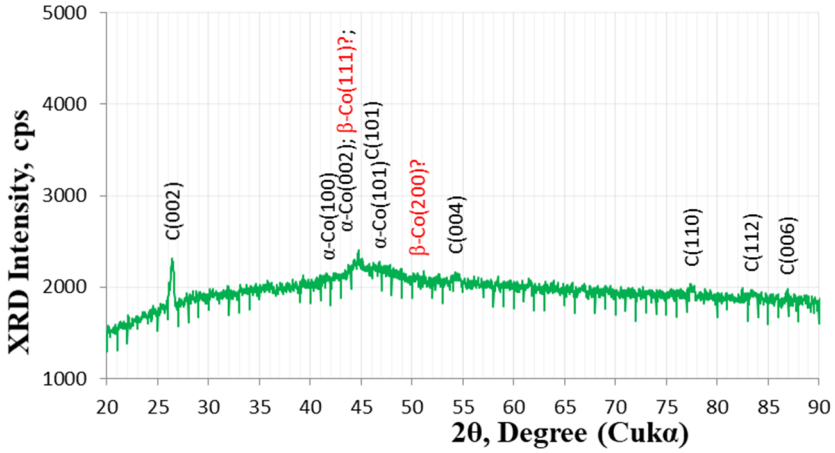

Fig. 8. X-ray diffractogram of the coating deposited on the graphite cathode using copper radiation; Electrodeposition from an electrolyte (mol L^{-1}): 0.1 $CoSO_4$+ 0.7 $C_6H_{11}Na0_7$ + 0.1 Na_2WO_4 + 0.5 $(NH_4)_2SO_4$ + 0.5 $MnSO_4$ + 0.007 But-2-yne-1,4-diol; pH 3.0; t= 30 ^{0}C; τ=20 min.

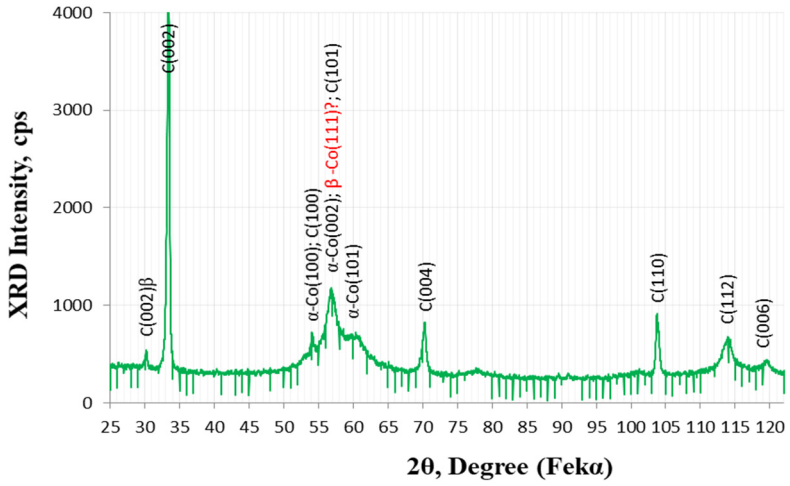

Fig. 9. X-ray diffractogram of the coating deposited from the same electrolyte (Fig. 8) on the graphite cathode using iron radiation.

Polarization study of Co-W coatings containing manganese. The corrosion-electrochemical behavior of the coatings was studied in a 3.5% NaCl aerated solution. Upon immersion of the electrodeposited coating (on the graphite cathode), its corrosion potential (E_{cor}) stabilized at -0.530 V vs. Ag/AgCl, gradually shifting ~5-8 mV positively over 12 hours due to active corrosion of Co and Mn. Atomic absorption spectroscopy confirmed Co^{2+} and Mn^{2+} release into the solution.

The initial E_{cor} (-0.530 V) closely matches the standard potential of Co^{2+}/Co ($E° = -0.277$ V vs. SHE). The anodic region of the polarization curve (Fig. 10, curve b) reveals active dissolution of the alloy, with Co and Mn oxidizing to soluble species (Co^{2+}, Mn^{2+}).

As the anodic potential increases, the surface concentration of active components (Co/Mn) decreases, slowing the anodic dissolution process. At higher potentials, the surface becomes predominantly covered by a tungsten-rich black layer, marked by the appearance of a passivation region on the polarization curve.

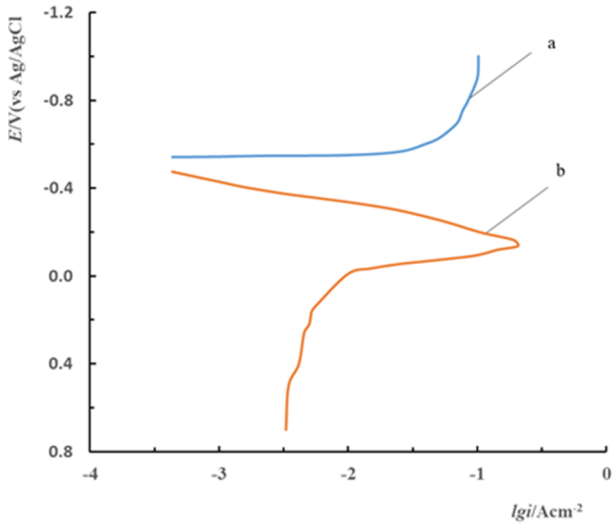

Fig. 10. Potentiodynamic (10 mV s^{-1}) cathodic (a) - anodic (b) polarization curves recorded on a manganese-containing Co-W coating electrodeposited on a graphite electrode in an aerated solution of 3.5% NaCl; t=30 °C

Polarization data indicate that Mn-containing Co-W coatings exhibit poor corrosion stability. However, after selective dissolution of active components (Co/Mn), the residual tungsten layer demonstrates passivation behavior, providing corrosion protection to the substrate material.

Conclusions

1. Brightly colored Co-Mn coatings (ω(Co):ω(Mn) = 1:1) with a current efficiency of 50% and a thickness of 32-36 μm were obtained from an electrolyte containing cobalt-manganese sulfate (T=25°C, pH 5.5), without any organic complexing agent, under constant current electrolysis conditions. The coating can be used to obtain an anti-corrosion protective layer of spinel-$(Mn,Co)_3O_4$ on steel using a known method.
2. CV curves recorded in electrolytes containing cobalt-manganese sulfates, sodium tungstate, and mixtures of non-toxic organic complexing agents (malic acid, sodium gluconate, sodium citrate-malic acid, and sodium citrate-EDTA) are characterized by a increase in current density at high negative cathodic potentials, which is associated with the electrodeposition of manganese-containing Co-W coatings and the simultaneous evolution of hydrogen gas, with current efficiency ranging from 91-95%.
3. Under constant current electrolysis conditions, the coatings obtained from electrolytes containing all organic complexing agents at cathodic current densities ranging from 0.05 to 0.25 $A \cdot cm^{-2}$ are shiny, relatively thin (approximately 5 μm), and exhibit high adhesion to the electrode; however, current efficiency decreases with increasing electrolysis duration (τ>20 min). At current densities above 0.25 $A \cdot cm^{-2}$, the coatings exhibit poor quality; all coatings contain oxygen. High-resolution SEM images show an uneven distribution of the alloy components and the presence of microcracks.

4. In an electrolyte containing a sodium citrate-EDTA complexing agent mixture at pH 3.5, increasing cathodic current density leads to a decrease in W content from 3 at.% to 1.5 at.%, and an increase in Mn content from 2 at.% to 5 at.%, while Co and O contents remain nearly unchanged at 55 at.% and 38 at.%, respectively. At pH 5.5, increasing current density results in increased Co content from 24 at.% to 59 at.%, increased Mn content from 1.78 at.% to 2.27 at.%, but decreased O content from 69 at.% to 34 at.%, while W content remains nearly unchanged at 3.6 at.%.
5. X-ray structural analysis reveals that manganese-containing Co-W coatings are most likely a solid solution of amorphous α-Co, in which W and Mn are randomly dissolved.
6. The corrosion potential of the manganese-containing Co-W coating obtained by electrodeposition on a graphite cathode in a 3.5% NaCl aerated solution is E_{cor} = -0.530 V (Ag/AgCl). During corrosion, cobalt and manganese are released from the coating into the solution. The anodic polarization curve exhibits zones of active dissolution, retardation, and passivation. The passivation zone results from the remaining tungsten layer after anodic dissolution of Co and Mn.

Acknowledgments

The work was supported by Shota Rustaveli National Science Foundation of Georgia (SRNSFG), Grant number: FR-22-11993

References

1. Bozzini B., Accardi V., Cavallotti P.L., Pavan F. Electrodeposition and plastic behavior of low-manganese zinc-manganese alloy coatings for automotive applications. *Met. Finish.* 1999, **Vol. 97(5),** p. 33-42. DOI:10.1016/S0026-0576(00)80031-8
2. Abd El Rehim S.S., Ibrahim M.A.M., Dankeria M.M., Emad M. Electrodeposition of Amorphous Cobalt-manganese Alloys on to steel from Gluconate Bathes. *Trans IMF*. 2002, **Vol. 80(3),** p.105-109. DOI: 10.1080/00202967.2002.11871444
3. Muller C., Sarret M., Andreu T. Electrodeposition of Zn-Mn alloys at low current densities. *J. Electrochem. Soc*. 2002, **Vol. 149 (11),** p. C600—C606. DOI: 10.1149/1.1512668
4. Muller C., Sarret M., Andreu T. Electrodeposition of Zn-Mn alloys using pulse plating. *J. Electrochem. Soc*. 2003, **Vol. 150 (11)**, p. C772-C776. DOI: 10.1149/1.1614270
5. Boshkov N., Petrov K., Vitkiva S. Corrosion products of zing-manganese coatings, part III: double-protective action of manganese. *Met. Finish*. 2002, **Vol. 100**, p. 98-102. DOI: 10.1016/S0026-0576(02)80445-7
6. Boshkov N., Petrov K., Vitkiva S., Raichevsky G. Galvanic alloys Zn-Mn composition of the corrosion products and their protective ability in sulfate containing medium. *Surf. Coat. Technol.* 2005, **Vol. 194**, p. 276-282. DOI: 10.1016/j.surfcoat.2004.09.016
7. Sylla D., Savall C., Gadouleau M., Rebere C., Creus J., Refait Ph. Electrodeposition of Zn-Mn alloys on steel using an alkaline pyrophosphate based electrolytic bath. *Surf. Coat. Technol.* 2005, **Vol. 200**, p. 2137-2145. DOI: 10.1016/j.surfcoat.2004.11.020
8. Ganesan S., Prabhu G., Popov B.N. Electrodeposition and characterization of Zn-Mn coatings for corrosion protection. *Surf. Coat. Technol*. 2014**, Vol. 2381**, p. 43-151. DOI: 10.1016/j.surfcoat.2013.10.062
9. Bedir M., Korkmaz D., Bakkaloglu O.F., Oztas M., Karahan I.H., Haciibrahimoglu M.Y. Effect of pH values on the characterization of electrodefosited Zn-Mn coatings in chloride based acidic environment. *Int. J. Electochem. Sci*. 2015, **Vol. 10,** p. 4513-4522. DOI: 10.1016/S1452-3981(23)06641-5
10. Tsurtsumia G., Koiava N., Gogoli D., Kakhniashvili I., Lejava T., Jokhadze N., Kemoklidze E. Study of Influence of the Electrolysis Parameters on Mn-Zn, Mn-Cu and Mn-Cu-Zn Alloys Coatings from Electrolytes Containing Complexing Ligands. *J. Chem. Chem. Eng***.** 2016, **Vol. 1**,

p. 13-27. DOI:10.17265/1934-7375/2016.01.003.
11. Gogoli D., Tsurtsumia G. Electrodeposition of Mn-Zn Alloy Coatings with high manganese content from Sulfate-EDTA solution in the presence of sodium selenite additive. *Res. J. of Pharmaceutical, Biological and Chemical Sciences*, 2018, **Vol. 9(4),** p.1678-1686.
12. Gogoli D., Tsurtsumia G. Composition and Morphologies of Mn-Ni and Mn-Ni-Cu Coatings Electrodeposited from Solution Containing Complexing Ligands EDTA and NTA. *Chemical Problems***,** 2019, **Vol. 17(2)**, p. 205-215. DOI: 10.32737/2221-8688-2019-2-205-215.
13. Gong J., Zangari G. Increased metallic character of electrodeposited Mn coatings using metal ion additives. *Electrochem. and Solid-State Letters*. 2004, **Vol. 7(9),** p. C91-C97. DOI: 10.1149/1.1774972
14. Gong J., Zangari G. Electrodeposition and characterization of sacrificial copper-manganese alloy coating. *J. Electrochem. Soc*. 2004**, Vol. 151(5),** p. C297-C306. DOI: 10.1149/1.1683618
15. Tsurtsumia G., Gogoli D., Koiava N., Kakhniashvili I., Jokhadze N., Lezhava T., Nioradze N., Tatishvili D. Characterization of Electrodeposited Mn-Cu-Zn Coating for Corrosion Protection. Current Topics and Emerging Issues in Materials Sciences. *Edited by Dr. Ho Soon Min*. 2023, **Vol. 1**, p. 97-107. DOI: 10.9734/bpi/cteims/v1/5158C
16. Wu J., Jiang Y., Jonson C., Liu X. DC electrodeposition of Mn-Co alloys on stainless steels for SOFC interconnect application. *J. Power Sources*, 2008, **Vol. 177**, p. 376-385. DOI: 10.1016/J.jpowsour.2007.11.075.
17. Wu J., Jonson C.D., Jiang Y., Gemmen R.S., Liu X. Pulse plating of Mn-Co alloys for SOFC interconnect application. *Electrochim. Acta*. 2008, **Vol. 54**, p. 793-800. DOI: 10.1016/J.electacta.2008.06.057.
18. Ebrahimifar H., Zandrahimi M. Influence of electrodeposition parameters on the characteristics of Mn-Co coatings on Crofer 22 APU ferritic stainless steel. *Bull. Mater. Sci.,* 2017, **Vol. 40 (6),** p. 1273-1283. DOI: 10.1007/s12034-017-1473-2.
19. Zhu J.H., Chesson D.A., Yu Y.T. Revew-(Mn, Co)$_3$O$_4$-Based Spinels for SOFC interconnect couthing application. *J. Electrochem. Soc.* 2021, **Vol. 168(11),** 114519. DOI: 10.1149/1945-7111/ac3a29.
20. Weston D.P., Shipway P.H., Harris S.J., Ching M.K. Friction and Sliding Wear Behaviour of Electrodeposited Cobalt and Cobalt-Tungsten Alloy Coatings for Replacement of Electrodeposited Chromium. *Wear.* 2009, **Vol. 267**, p. 934-943. DOI: 10.1016/j.wear.2009.01.006
21. Weston D.P., Harris S.J., Capel H., Ahmed N., Shipway P.H., Yellup J.N. Nanostructured Co-W Coatings Produced by Electrodeposition to Replace Hard Cr on Aerospace Components. *Trans. Inst. Met. Finish*. 2010, **Vol. 88(1),** p. 47-56. DOI: 10.1179/174591909X12596810686490
22. Brenner A. *Principles and Practice. Electrodeposition of alloys.* Academic Press. New York. USA. London. UK: 1963.
23. Eliaz N., Gileadi E. *Induced Codeposition of Alloys of Tungsten, Molybdenum and Rhenium with Transition Metals*. In: Vayenas C.G., White R.E., Gamboa-Aldeco M.E. (eds) Modern Aspects of Electrochemistry. Modern Aspects of Electrochemistry. 2008. **Vol. 42**. Springer. New York. NY. DOI: 10.1007/978-0-387-49489-0_4
24. Tsyntsaru N., Cesiulis H., Donten M., Sort J., Pelliccer E., Podlaha-Murphy E.J. Modern Trends in Tungsten Alloys Electrodeposition with Iron Group Metals. *Surf. Eng. Appl. Electrochem*. 2012, **Vol. 48(6),** p. 491–520. DOI: 10.3103/S1068375512060038.
25. Tsyntsaru N., Belevsky S., Dikusar A., Celis J.-P. Trobological behaviour of electrodeposited Cobalt-Tungsten coatings. *Trans. Inst. Met. Finish*. 2008, **Vol. 86(6),** p. 301-307. DOI: 10.1179/174591908X371131
26. Silkin S.A., Belevski S.S., Tsintsaru N.I., Shul'man A.I., Shchuplykov A.N, Dikusar A.I. Influence of Long-Term operation of electrolytes on the composition, morphology, and mechanical properties of surface produced at deposition of Co-W coatings from citrate solutions. *Surf. Eng.*

Appl. Electrochem. 2009, **Vol. 45(1),** p. 1-12. DOI: 10.3103/S1068375509010013
27. Belevskii S.S., Cesiulis H., Tsyntsaru N.I., Dikusar A.I. The role of mass transfer in the formation of the composition and structure of CoW coatings electrodeposited from citrate solutions. *Surf. Eng. Appl. Electrochem***.** 2010, **Vol. 46**, p. 570–578. DOI: 10.3103/S1068375510060050
28. Tsyntsaru N., Belevsky S., Dikusar A., Celis J.-P. Tribological behavior of electrodeposited cobalt-tungsten coatings: dependence on current parameters. *Trans. Inst. Met. Finish*. 2008, **Vol. 86**, p. 301–307. DOI: 10.1179/174591908X371131
29. Tsyntsaru N., Cesiulis H., Donten M., Sorte J., Pellicer E., Podlaha-Murphy E.J. Modern trends in tungsten alloys electrodeposition with iron group metals. *Surf. Eng. Appl. Electrochem*. 2012, **Vol. 48**, p. 491–520. DOI:10.3103/S1068375512060038
30. Ibrahim M.A.M., El Rehim S.S.A., Moussa S.O. Electrodeposition of noncrystalline cobalt–tungsten alloys from citrate electrolytes. *J. Appl. Electrochem*. 2003, **Vol. 33**, p. 627–633. DOI:10.1023/A:1024916903544.
31. Vernickaite E., Tsyntsaru N., Sobczak K., Cesiulis H. Electrodeposited tungsten-rich Ni-W, Co-W and Fe-W cathodes for efficient hydrogen evolution in alkaline medium. *Electrochim. Acta.* 2019, **Vol. 318**, p. 597–606. DOI: 10.1016/j.electacta.2019.06.087.
32. Tsyntsaru N., Cesiulis H., Budreika A., Ye X., Juskenas R., Celis J.-P. The effect of electrodeposition conditions and post-annealing on nanostructure of Co–W coatings. *Surf. Coat. Technol*. 2012, **Vol. 206**, p. 4262–4269. DOI: 10.1016/j.surfcoat.2012.04.036.
33. Vernickaite E., Tsyntsaru N., Cesiulis H. Electrochemical co-deposition of tungsten with cobalt and copper: Peculiarities of binary and ternary alloys coatings formation. *Surf. Coat. Technol.* 2016, **Vol. 307**, p. 1341–1349. DOI: 10.1016/j.surfcoat.2016.07.025
34. Fan C., Piron D.L., Sleb A., Paradis P. Study of Electrodeposited Nickel-Molybdenum, Nickel-Tungsten, Cobalt-Molybdenum, and Cobalt-Tungsten as Hydrogen Electrodes in Alkaline Water Electrolysis. *J. Electrochem. Soc*. 1994, **Vol. 141**, p. 382–387. DOI: 10.1149/1.2054736.
35. Vernickaite E., Tsyntsaru N., Sobczak K., Cesiulis H. Electrodeposited tungsten-rich Ni-W, Co-W and Fe-W cathodes for efficient hydrogen evolution in alkaline medium. *Electrochim. Acta.* 2019, **Vol. 318**, p. 597–606. DOI: 10.1016/j.electacta.2019.06.087.
36. Laszczyńska A. Electrodeposited alloy electrodes in the Co-W-Mo system as highly efficient catalysts for hydrogen production from alkaline water electrolysis. *Mater. Chem. Phys*. 2024, **Vol. 314**, 128876. DOI:1016/j.matchemphys.2023.128876.
37. Sulitanu N. *Electroplating and Electroless Deposition of Nanostructured Magnetic Thin Films*. in: Tsakalakos T., Ovidko I.A., Vasudevan A.K. (eds). Conference paper. Nanostructures: Synthesis, Functional Properties and Applications. NATO Science Series, Springer, Dordrecht. 2003, **Vol. 128**, p. 511-532. DOI: 10.1007/978-94-007-1019-1_30
38. Belevskii S.S., Yushenko S.P., Dikusar A.I. Anomalous electrodeposition of Co-W coatings from a Ctrate electrolyte Due to the Formation of multinuclear heterometallic complexes in the Solution. *Surf. Eng. Appl. Electrochem*. 2012, **Vol. 48(1),** p. 97-98. DOI: 10.3103/S1068375512010036
39. Shulman A.I., Belevskii S.S., Yushenko S.P., Dikusar A.I. Complexation as a factor of the formation of composition coated of Co-W, electrodeposited from a gluconate electrolyte. *J. Electronic metal processing (Russian)*, 2014, **Vol. 50(1),** p. 8-1.
40. Gamburg D., Zangari G. *Theory and Practice of Metal Electrodeposition*. Springer New York. 2011.